Eur. Phys. J. A (2016) **52**: 21
DOI 10.1140/epja/i2016-16021-6

THE EUROPEAN PHYSICAL JOURNAL A

Regular Article – Theoretical Physics

Hyperon-hyperon interactions with the Nijmegen ESC08 model*

Th.A. Rijken[1,a] and H.-J. Schulze[2]

[1] IMAPP, Radboud University, 6525 AJ Nijmegen, The Netherlands
[2] INFN Sezione di Catania, Dipartimento di Fisica, Università di Catania, Via Santa Sofia 64, I-95123 Catania, Italy

Received: 23 September 2015
Published online: 8 February 2016

Communicated by D. Blaschke

Abstract. We discuss the properties of the hyperon-hyperon interactions in the recent Nijmegen ESC08 potential, in particular the importance of the coupled-channel structure and related existence of bound states. Brueckner-Hartree-Fock calculations of hypernuclear matter employing these interactions are presented and the structure of hyperon (neutron) stars within this approach is computed. Low maximum masses are found.

1 Introduction

This article is a follow up of our paper on the maximum mass of hyperon stars with the Nijmegen ESC08 model [1]. In the present work we supplement the ESC08b nucleon-hyperon (NY) $S = -1$ potentials [2–5] with the recently developed ESC08c hyperon-hyperon (YY) $S = -2$ interactions [6]. This implies to study also the Ξ hyperon apart from the Λ and Σ hyperons.

The recent discovery of two-solar-mass neutron stars (NS) [7,8] is a very important issue, which makes theoretical investigations of the inner structure of such compact stellar objects timely. Hyperons are expected to appear in beta-stable matter already at relatively low densities of about twice the nuclear saturation density. It is well known that the appearance of "exotic" components (such as hyperons, mesons, quarks) in beta-stable NS matter might lead to a substantial softening of the equation of state (EOS) and reduce the theoretical maximum mass of the star below the observed masses [9–13].

It was pointed out in previous works that there exists an important self-regulating compensation mechanism that always leads to rather low neutron star masses by the appearance of hyperons. Namely, without the introduction of some universal repulsive N-baryon force ($N > 2$), a stiffer nucleonic EOS will cause an earlier onset of hyperons and thus a stronger softening effect, and vice versa. The same is true for individual components of the hyperonic EOS, *e.g.*, a more repulsive $N\Sigma$ interaction is expected to lead to an earlier onset of the Λ, etc. This was reaffirmed in [1], and it is of particular interest to see this mechanism at work in the more complete new study presented here.

To carry out high-quality calculations of hypernuclear matter and the corresponding hyperon star structure, it is necessary to use baryon-baryon (BB) interactions strongly constrained by independent experimental information on the hyperon-nucleon interactions. Then, confronting such accurate and realistic theoretical calculations with observational data, one might be able to draw conclusions with regard to the presence of hyperons in stellar matter, and thus on the features of the underlying fundamental interactions.

This requires advanced microscopic many-body approaches to the EOS of (hyper)nuclear matter. The, by now classic, Brueckner theory has in recent years seen solid progress regarding the convergence of the Brueckner-Bethe-Goldstone (BBG) expansion. Namely, the two-hole-line truncation, the so-called Brueckner-Hartree-Fock (BHF) approximation, gives a EOS which is insensitive to the choice of the auxiliary potential, provided one makes the continuous choice of the single-particle (s.p.) potential [14–16].

Like in [1], also this paper uses the non-relativistic BBG expansion, and studies the possible appearance of hyperons in NS matter within the BHF theoretical many-body approach, continuing several earlier publications [17–25]. The fundamental input of these parameter-free calculations are realistic potentials in the nucleon-nucleon (NN), NY, and YY sectors, supplemented by three-body forces (TBF), which at least in the NN case are required in order to ensure a correct saturation point of nuclear matter.

* Contribution to the Topical Issue on "Exotic matter in neutron stars" edited by David Blaschke, Jürgen Schaffner-Bielich, Hans-Josef Schulze.

[a] e-mail: T.Rijken@science.ru.nl

At present, several high-quality NN potentials are available for theoretical calculation, together with nuclear TBF which have been either determined empirically by fitting the saturation point of nuclear matter [26–28], or constructed in a microscopic way, compatible with the two-body potential that is used [29–32]. There exist also several NY potentials fitted to scattering data, while the potentials in the YY sector and the TBF involving hyperons have presently to be considered rather uncertain or unknown, which is basically due to the lack of appropriate experimental data and/or the great difficulties of their theoretical analysis.

In this paper the BHF calculations of hypernuclear matter are performed with the Argonne V_{18} NN potential [33], together with the microscopic nuclear TBF [32], which is more repulsive than the UIX TBF [34,35] used before. Previous papers used the Nijmegen NSC89 [36], or NSC97 [37], or ESC08b [1] NY potentials. Very low maximum masses of hyperon stars, below $1.4M_{\odot}$, were always found [1,21,22].

The purpose of this work is to extend those calculations by employing the recently developed ESC08c YY potentials [6]. The chief difference with [1] is thus the inclusion of the $(S=-2)$ $\Lambda\Lambda, N\Xi, \Sigma\Lambda, \Sigma\Sigma$ channels. The interaction in the $\Lambda\Lambda$ channels is weak, and the $N\Xi$ interaction is repulsive in the ${}^1S_0$ and attractive in the ${}^3S_1$ states, leading to a moderate well depth $U_{\Xi} \approx -8\,\mathrm{MeV}$. The attraction in the ${}^3S_1$ state is due to the tensor force, leading to a weakly bound strangeness $S=-2$ deuteron with binding energy $B = 1.56\,\mathrm{MeV}$.

The content of this paper is as follows: In sect. 2 we introduce the features of the newest Nijmegen ESC08 potential and the role of the constituent quark model and multi-pomeron exchange, with particular attention to the YY channels. In sect. 3 the BHF approach to neutron star matter is briefly reviewed. Section 4 presents numerical results, including parametrizations of the energy density function, and the results on the NS structure. In sect. 5 conclusions and future prospects are given.

2 The Nijmegen ESC08 potential

The extended soft-core ESC08 models [4–6] for BB interactions of the SU(3) flavor octet of baryons (N, Λ, Σ, and Ξ) provide a presentation of the forces in terms of i) meson exchange, using generalized soft-core Yukawa functions; ii) multiple gluon exchange (pomeron and odderon); and iii) structural effects due to the quark core of the baryons, the so-called Pauli blocking. Relativistic effects are included via expansion in inverse baryon masses $1/m_B$. The ESC meson-exchange interactions contain local and non-local potentials due to a) one-boson exchanges (OBE), which are members of nonets of pseudoscalar, vector, scalar, and axial mesons; b) pomeron and odderon exchanges; c) two pseudoscalar exchanges (TME); and d) meson pair exchanges (MPE). The OBE and MPE vertices are regulated by gaussian form factors, where the assignment of the cut-off masses for the baryon-baryon-meson (BBM) vertices depends on the SU(3) classification of the exchanged mesons for OBE, and a similar scheme for MPE.

The ESC models describe the NN, NY, and YY interactions in a unified way using broken SU(3) symmetry. This serves to connect the NN, NY, and YY channels and is utilized to make a simultaneous fit to the NN and NY data with a restricted set ($\lesssim 20$) of free coupling constants, etc., see [4–6] for details. In particular, the BBM coupling constants are calculated via SU(3), using, together with the meson mixing angles, the fitted constants in the NN $\oplus$ NY analysis as input. In ESC08 no breaking of SU(3) is assumed for the couplings, with the exception of the following cases: i) NN, the isospin breaking for the ρ meson is exploited phenomenologically in order to account for the difference between ${}^1S_0(pp)$, ${}^1S_0(np)$, and ${}^1S_0(nn)$; ii) charge symmetry breaking in the $p\Lambda$ and $n\Lambda$ channels. In the latter case the SU(2) isospin breaking is included in the OBE, TME, and MPE potentials.

In ref. [1] the results with the ESC08b NY model [4, 5] are described. In this paper the improved ESC08c model [6] is used as a basis for the YY interactions. With this model excellent results are achieved for the NN and NY data: i) For the selected 4233 NN data of the Nijmegen phase shift analysis [38] with energies $0 \le T_{\mathrm{lab}} \le 350\,\mathrm{MeV}$ a χ^2/data=1.08 is realized, which is remarkably close to that of the multi-energy phase shift analysis. ii) For the set of 52 NY $S=-1$ data, also used in previous Nijmegen studies, in ESC08b a χ^2/data ≈ 1.07 was reached, with no bound states in these NY channels. As regards to the well depth U_{Λ}, there is some overbinding, making room for, *e.g.*, three-body repulsion. iii) For YY there is a weak $\Lambda\Lambda$ attraction, *e.g.*, in ESC08 $|a_{\Lambda\Lambda}({}^1S_0)| < 1.0$, which matches experimental indication from the Nagara event [39]. Among the predictions for the $S=-2$ sector $(\Lambda\Lambda, N\Xi, \Lambda\Sigma, \Sigma\Sigma)$ are the existence of bound states in the $N\Xi({}^3SD_1, T=1)$ channels.

2.1 Constituent quark model and multi-gluon exchange

In the ESC models the coupling constants, and the $F/(F+D)$ ratios as well, can be understood in the framework of the constituent quark model (CQM), as generated by folding the quark-antiquark pair creation processes with the ground-state 3-quark baryon wave functions, see, *e.g.*, [6]. Furthermore, it turns out that in the CQM the meson-exchange BB potentials can be reproduced by folding meson exchange between the constituent quarks. Thereby the corresponding meson-quark-quark vertices are determined, which defines in principle (part of) the quark-quark interactions [40].

In some G-matrix applications of the ESC model [41–43] an important role is played by multi-gluon interactions in the form of a (phenomenological) repulsive multi-pomeron TBF. Since the gluons are flavor blind, the same holds for the pomeron and therefore this repulsion is universal. The multi-pomeron exchange has a clear QCD origin and must be operative between quarks as well. This enables the ESC models to produce a satisfactory nuclear saturation curve, and good well depths U_{Λ}, U_{Σ}, and U_{Ξ}.

$$\boldsymbol{V}^{Q=0} = \begin{pmatrix} V^0_{aa} & s_2 V^0_{ab} & -s_2 V^0_{ab} & 0 & -s_3 V^0_{ad} & s_3 V^0_{ad}/s_2 \\ . & [V^1_{bb}+V^0_{bb}]/2 & [V^1_{bb}-V^0_{bb}]/2 & s_2 V^1_{bc} & -s_6 V^0_{bd} & s_3 V^0_{bd} - s_2 V^1_{bd} \\ . & . & [V^1_{bb}+V^0_{bb}]/2 & s_2 V^1_{bc} & s_6 V^0_{bd} & -s_3 V^0_{bd} - s_2 V^1_{bd} \\ . & . & . & V^1_{cc} & 0 & -V^1_{cd} \\ . & . & . & . & [V^0_{dd}+2V^2_{dd}]/3 & [V^2_{dd}-V^0_{dd}]/(3s_2) \\ . & . & . & . & . & [2V^0_{dd}+3V^1_{dd}+V^2_{dd}]/3 \end{pmatrix}, \tag{4}$$

Thus, the ESC08 model parameters are compatible with the CQM, and give at the same time an excellent description of the NN, NY, and YY data. Moreover, the nuclear saturation curve is reproduced. Therefore, this BB potential model, combined with the BHF techniques using the continuous choice, provides a good basis for the calculation of both symmetric and neutron star matter.

The free parameters in the ESC models are in principle fitted to the NN and NY scattering data for the $S = 0$ and $S = -1$ sectors. Constraints used from the $S = -2$ channels is the information from the Nagara event [39], and the attractive well depth $U_\Xi \approx -(8\text{–}10)\,\mathrm{MeV}$ [6,44, 45]. This information is a rather minimal one, and the $S = -2$ results are almost parameter-free predictions. Below we review briefly some properties of the ESC08c model in the $S = -2$ channels.

2.2 Properties of the YY interaction

The $S = -2$; $I = 0, 1, 2$ potentials V^I_{ij} ($i, j = \Lambda\Lambda$, $N\Xi$, $\Lambda\Sigma$, $\Sigma\Sigma$) are constructed in the isospin basis for the seven independent channels

$$I = 0: \quad (\Lambda\Lambda, N\Xi, \Sigma\Sigma) \equiv (a, b, d), \tag{1a}$$
$$I = 1: \quad (N\Xi, \Lambda\Sigma, \Sigma\Sigma) \equiv (b, c, d), \tag{1b}$$
$$I = 2: \quad (\Sigma\Sigma) \equiv (d), \tag{1c}$$

defining $[a, b, c, d] = [\Lambda\Lambda, N\Xi, \Lambda\Sigma, \Sigma\Sigma]$. However, for the calculation of isospin-asymmetric hypernuclear matter, the particle basis

$$Q = 0: \quad (\Lambda\Lambda, n\Xi^0, p\Xi^-, \Lambda\Sigma^0, \Sigma^0\Sigma^0, \Sigma^-\Sigma^+), \tag{2a}$$
$$Q = 1: \quad (p\Xi^0, \Lambda\Sigma^+, \Sigma^0\Sigma^+), \tag{2b}$$
$$Q = 2: \quad (\Sigma^+\Sigma^+). \tag{2c}$$

has to be used with the following transformations

$$\boldsymbol{V}^{Q=1} = \begin{pmatrix} V^1_{bb} & V^1_{bc} & -V^1_{bd} \\ V^1_{cb} & V^1_{cc} & -V^1_{cd} \\ -V^1_{db} & -V^1_{dc} & V^1_{dd}+V^2_{dd} \end{pmatrix}, \tag{3}$$

see eq. (4) *above*

with the abbreviation $s_i \equiv \sqrt{1/i}$.

Table 1. Inverse scattering length and effective-range matrices at the $N\Xi$ threshold for $I = 0$, and the $\Lambda\Sigma$ threshold for $I = 1$. The order of the states $(1, 2)$ reads $\Lambda\Lambda(^1S_0), N\Xi(^1S_0)$ and $N\Xi(^1S_0), \Lambda\Sigma(^1S_0)$ for $I = 0$ and $I = 1$, respectively, and $N\Xi(^3S_1), N\Xi(^3D_1), \Lambda\Sigma(^3S_1)$ for $(1, 2, 3)$. The dimensions of the matrix elements are $\mathrm{fm}^{-1-l-l'}(A^{-1})$ and $\mathrm{fm}^{1-l-l'}(R)$.

	$N\Xi(I=0)$ threshold		$\Lambda\Sigma(I=1)$ threshold	
	A^{-1}	R	A^{-1}	R
11	0.472	13.001	0.062	11.774
12	1.591	2.088	−1.436	9.744
22	0.870	3.276	−0.736	9.659
	$\Lambda\Sigma(I=1)$ threshold			
	A^{-1}	R		
11	1.302	1.454		
12	−9.122	18.305		
13	0.504	1.709		
22	239.128	−590.173		
23	4.252	−16.637		
33	1.030	1.540		

2.3 Effective-range parameters

The ESC08c low-energy parameters (in units of fm) are for $I = 0$,

$$a_{\Lambda\Lambda}(^1S_0) = -0.853, \quad r_{\Lambda\Lambda}(^1S_0) = 5.126, \tag{5a}$$
$$a_{N\Xi}(^3S_1) = -5.357, \quad r_{N\Xi}(^3S_1) = 1.434, \tag{5b}$$

for $I = 1$,

$$a_{N\Xi}(^1S_0) = 0.579, \quad r_{N\Xi}(^1S_0) = -2.521, \tag{5c}$$
$$a_{N\Xi}(^3S_1) = 4.911, \quad r_{N\Xi}(^3S_1) = 0.527, \tag{5d}$$

and for $I = 2$

$$a_{\Sigma^\pm\Sigma^\pm}(^1S_0) = 8.10\ (-0.65), \tag{5e}$$
$$r_{\Sigma^\pm\Sigma^\pm}(^1S_0) = -65.36\ (19.97). \tag{5f}$$

The values given in parentheses are without Coulomb interaction. The results at the $N\Xi$ and $\Lambda\Sigma$ thresholds are given in table 1.

The old experimental information seemed to indicate a separation energy $\Delta B_{\Lambda\Lambda} \approx 5\,\mathrm{MeV}$ of double-Λ hypernuclei, corresponding to a rather strong attractive $\Lambda\Lambda$ interaction. As a matter of fact the $\Lambda\Lambda$ $^1S_0$ scattering length based on such a value for $\Delta B_{\Lambda\Lambda}$ gives $a_{\Lambda\Lambda}(^1S_0) \approx -2.0\,\mathrm{fm}$.

Table 2. SU(3) content of the different interaction channels with total strangeness S and isospin I. The upper half refers to the space-spin symmetric states $^3S_1$, $^1P_1$, ^3D, ..., and the lower half to the space-spin antisymmetric states $^1S_0$, ^3P, $^1D_2$, ...

S	I	Channels	SU(3)-irreps
Space-spin symmetric			
0	0	NN	$\{10^*\}$
-1	1/2	ΛN, ΣN	$\{10^*\}$, $\{8\}_a$
	3/2	ΣN	$\{10\}$
-2	0	$N\Xi$	$\{8\}_a$
	1	$N\Xi$, $\Sigma\Sigma$	$\{10\}$, $\{10^*\}$, $\{8\}_a$
		$\Sigma\Lambda$	$\{10\}$, $\{10^*\}$
Space-spin antisymmetric			
0	1	NN	$\{27\}$
-1	1/2	ΛN, ΣN	$\{27\}$, $\{8\}_s$
	3/2	ΣN	$\{27\}$
-2	0	$\Lambda\Lambda$, $N\Xi$, $\Sigma\Sigma$	$\{27\}$, $\{8\}_s$, $\{1\}$
	1	$N\Xi$, $\Sigma\Lambda$	$\{27\}$, $\{8\}_s$
	2	$\Sigma\Sigma$	$\{27\}$

However, the experimental information and interpretation of the ground state levels of ${}^{\ 6}_{\Lambda\Lambda}$He, ${}^{10}_{\Lambda\Lambda}$Be, and ${}^{13}_{\Lambda\Lambda}$B [46] has been changed drastically. This because of the Nagara event [39], identified uniquely as ${}^{\ 6}_{\Lambda\Lambda}$He, which established that the $\Lambda\Lambda$ interaction is much weaker ($\Delta B_{\Lambda\Lambda} \approx 0.7\,\mathrm{MeV}$).

In the ESC models it is only possible to increase the attraction in the $\Lambda\Lambda$ channel by modifying the scalar-exchange potential. If the scalar mesons are viewed as being mainly $q\bar{q}$ states, one finds that the (attractive) scalar-exchange part of the interaction in the various channels satisfies $|V_{\Lambda\Lambda}| < |V_{N\Lambda}| < |V_{NN}|$, suggesting indeed a rather weak $\Lambda\Lambda$ potential. The ESC fits to the NY scattering data [47] give values for the scalar-meson mixing angle, which seem to point to almost ideal mixing for the scalars as $q\bar{q}$ states. This is also true for the Nijmegen OBE models NSC89/NSC97. In these models an increased attraction in the $\Lambda\Lambda$ channel gives rise to (experimentally unobserved) deeply bound states in the $N\Lambda$ channel. As one sees from the values of $a_{\Lambda\Lambda}(^1S_0)$ in the ESC08c model, we can produce the apparently required attraction in the $\Lambda\Lambda$ interaction without giving rise to $N\Lambda$ bound states.

For the $N\Xi$ channels one sees from (5c) and (5d) that the $^1S_0(I=1)$ is rather repulsive and that the $^3S_1$ waves are attractive for $I = 0, 1$. The latter is needed in order to have a reasonable attractive Ξ-nucleus well depth.

2.4 Deuteron state in $N\Xi(^3SD_1, I = 1)$

A discussion of the possible bound states, using the SU(3) content of the different $S = 0, -1, -2$ channels is given in [37]. For a general orientation, we list in table 2 all the irreps to which the various BB channels belong. In ESC08c we find a D^* deuteron with isospin $I = 1$ and strangeness $S = -2$, belonging to the $\{10^*\}$ SU(3) irrep,

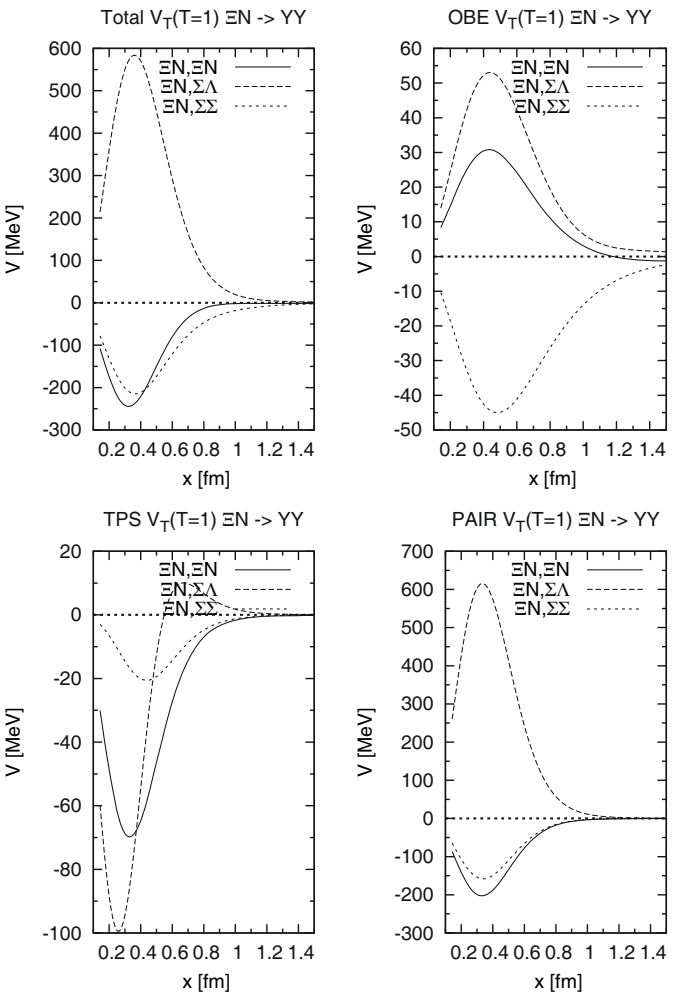

Fig. 1. $N\Xi(^3S_1, I = 1)$ tensor potentials.

which is a $N\Xi$ bound state in the $^3SD_1$ coupled partial wave. The occurrence of this deuteron-like bound state is rather natural, since it is caused by the presence of strong $N\Xi \to N\Xi, \Sigma\Lambda$ tensor forces, shown in fig. 1, similarly to the np deuteron. (In the $N\Lambda, N\Sigma$ system the tensor force leads to a virtual bound state below the $N\Sigma$ threshold, where a large cusp occurs.)

The calculated binding energy is $B(D^*) = 1.56\,\mathrm{MeV}$. So far, except for the np deuteron, no other BB bound states have been found experimentally. The search of the Rome-Saclay-Vanderbilt collaboration [48] was negative, but since D^* is a narrow state just below the $N\Xi$ threshold, the detection requires a very good experimental resolution.

2.5 Flavor-SU(3) irrep potentials

In fig. 2 the SU(3) irreps are displayed. The solid lines show averages of the SU(3)-irrep potentials in the particle basis. The dashed lines are the irrep potentials in an SU(3) limit, where $M_N = M_\Lambda = M_\Sigma = M_\Xi = 1115.6\,\mathrm{MeV}$, $m_\pi = m_K = m_\eta = m_{\eta'} = 410\,\mathrm{MeV}$, $m_\rho = m_{K^*} = m_\omega = m_\phi = 880\,\mathrm{MeV}$, and $m_{a_0} = m_\kappa = m_\sigma = m_{f_0'} = 880\,\mathrm{MeV}$.

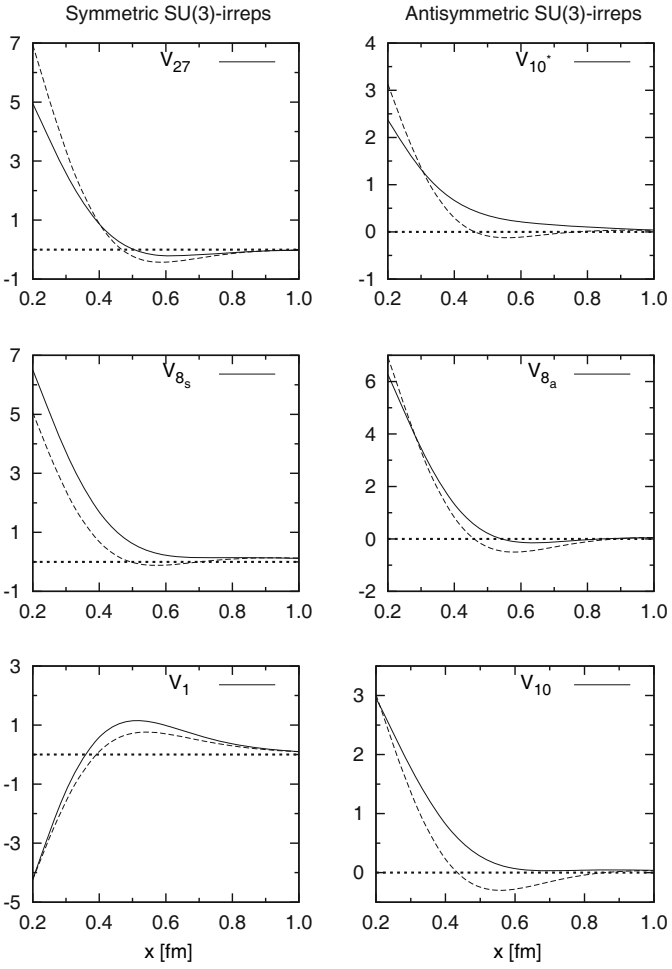

Fig. 2. Solid curves: average SU(3)-irrep potentials (in GeV) in the particle basis. Dashed curves: potentials with exact flavor SU(3) symmetry.

The Lattice QCD calculations of refs. [49,50] show qualitatively very similar results, with the exception of the SU(3)-singlet {1} irrep. Here the lattice potential is always attractive for $0 < r < \infty$, whereas in ESC08c there is an attractive pocket for $r \lesssim 0.5\,\mathrm{fm}$ and repulsion for $r \gtrsim 0.5\,\mathrm{fm}$. This is due to strong spin-spin potentials from pseudoscalar and vector exchange, which have zero volume integrals and consequently have a sign change. In the {1} irrep for the SU(3)-broken potential (solid line) there is no bound state, *i.e.*, no H particle [51]. This is in agreement with the experimental results up to now, see, *e.g.*, the recent $\Upsilon(1S, 2S)$-decay studies [52].

3 BHF approach to neutron star structure

In this section we give a short review of the BHF approach including hyperons, while detailed descriptions can be found in refs. [17–20].

The basic input quantities in the Bethe-Goldstone equation are the NN, NY, and YY potentials. In this work we use the Argonne V_{18} NN potential [33] supplemented by the microscopic TBF of refs. [29–32], and the ESC08 NY+YY potentials [6], that are well adapted to the existing experimental NY data.

With these potentials, the various G-matrices are evaluated by solving numerically the Bethe-Goldstone equation, which can be written in operator form as

$$G_{ab}[W] = V_{ab} + \sum_c \sum_{p,p'} V_{ac}|pp'\rangle \frac{Q_c}{W - E_c + i\varepsilon} \langle pp'|G_{cb}[W], \tag{6}$$

where the indices a, b, c indicate pairs of baryons, and the Pauli operator Q_c and energy E_c characterize the propagation of intermediate baryon pairs. The pair energy in a given channel $c = (B_1 B_2)$ is

$$E_{(B_1 B_2)} = T_{B_1}(k_{B_1}) + T_{B_2}(k_{B_2}) + U_{B_1}(k_{B_1}) + U_{B_2}(k_{B_2}), \tag{7}$$

with $T_B(k) = m_B + k^2/2m_B$, where the various s.p. potentials are given by

$$U_B(k) = \sum_{B'=n,p,\Lambda,\Sigma^-} U_B^{(B')}(k) \tag{8}$$

and are determined self-consistently from the G-matrices,

$$U_B^{(B')}(k) = \sum_{k'<k_F^{(B')}} \mathrm{Re}\langle kk'|G_{(BB')(BB')}[E_{(BB')}(k,k')]|kk'\rangle_A. \tag{9}$$

The coupled eqs. (6)–(9) define the BHF scheme with the continuous choice of the s.p. energies. It has been shown that with this choice the nuclear EOS can be calculated with good accuracy in the Brueckner two-hole-line approximation, because the results are quite close to the calculations which also include the three-hole-line contribution [14–16]. In contrast to the standard purely nucleonic case, the additional coupled-channel structure due to the hyperons renders the calculation quite time-consuming.

Once the different s.p. potentials are known, the total non-relativistic baryonic energy density ε can be evaluated:

$$\varepsilon = \sum_{B=n,p,\Lambda,\Sigma^-} \sum_{k<k_F^{(B)}} \left[T_B(k) + \frac{1}{2} U_B(k) \right] = \varepsilon_N + \varepsilon_Y, \tag{10}$$

where

$$\varepsilon_N = \sum_{N,N'=n,p} \sum_{k<k_F^{(N)}} \left[T_N + \frac{1}{2} U_N^{(N')} \right](k), \tag{11a}$$

$$\varepsilon_Y = \sum_{\substack{Y,Y'=\Lambda,\Sigma^- \\ N=n,p}} \sum_{k<k_F^{(Y)}} \left[T_Y + U_Y^{(N)} + \frac{1}{2} U_Y^{(Y')} \right](k). \tag{11b}$$

Using the baryonic energy density eq. (10), and adding the contributions of the non-interacting leptons, the various chemical potentials $\mu_i = \partial\varepsilon/\partial\rho_i$ (of the species $i = n, p, \Lambda, \Sigma^-, e, \mu$) can be computed straightforwardly and the equations for beta equilibrium, $\mu_i = b_i\mu_n - q_i\mu_e$ (b_i and q_i denoting baryon number and charge of species i),

and charge neutrality, $\sum_i \rho_i q_i = 0$, allow one to determine the equilibrium composition $\{\rho_i(\rho)\}$ at given baryon density $\rho = \rho_n + \rho_p + \rho_\Lambda + \rho_\Sigma$, and finally the EOS:

$$p(\rho) = \rho^2 \frac{\mathrm{d}}{\mathrm{d}\rho} \frac{\varepsilon(\{\rho_i(\rho)\})}{\rho} = \rho \frac{\mathrm{d}\varepsilon}{\mathrm{d}\rho} - \varepsilon. \tag{12}$$

Knowing the EOS, the equilibrium configurations of static NS are obtained by solving the Tolman-Oppenheimer-Volkov equations [9–13] for the pressure $p(r)$ and the enclosed mass $m(r)$,

$$\frac{\mathrm{d}p}{\mathrm{d}r} = -\frac{Gm\varepsilon}{r^2} \frac{(1+p/\varepsilon)(1+4\pi r^3 p/m)}{1-2Gm/r}, \tag{13a}$$

$$\frac{\mathrm{d}m}{\mathrm{d}r} = 4\pi r^2 \varepsilon, \tag{13b}$$

being G the gravitational constant. Starting with a central mass density $\varepsilon(r=0) \equiv \varepsilon_c$, one integrates out until the surface density equals that of iron. This gives the stellar radius R and its gravitational mass $M = m(R)$. For the description of the NS crust, we join the hadronic EOS with those of Negele and Vautherin [53] in the medium-density regime, and those by Feynman-Metropolis-Teller [54] and Baym-Pethick-Sutherland [55] for the outer crust.

4 Results

We now present the numerical results obtained within the BHF formalism for hypernuclear matter and NS structure, as detailed before.

4.1 Parametrization of the energy density function

The large number of degrees of freedom (4 partial densities for $n, p, \Lambda, \Sigma \equiv \Sigma^-$) renders inconvenient the use of the resulting hypernuclear EOS in tabular form. We therefore approximate the numerical results by a sufficiently accurate analytical parametrization. We find that the following functional form provides an excellent fit of the numerical data for the energy density, eq. (10), in the required ranges of nucleon density ($0.1\,\mathrm{fm}^{-3} \lesssim \rho_N \lesssim 0.8\,\mathrm{fm}^{-3}$), proton fraction ($0.0 \le \rho_p/\rho_N \le 0.5$), and hyperon fractions ($0 \le \rho_\Lambda/\rho_N \le 0.8$, $0 \le \rho_\Sigma/\rho_N \le 0.5$):

$$\begin{aligned}\varepsilon(\rho_n,\rho_p,\rho_\Lambda,\rho_\Sigma) &= E_N \rho_N \\ &+ (E_\Lambda + E_{\Lambda\Lambda} + E_{\Lambda\Sigma})\,\rho_\Lambda + \frac{C}{2m_\Lambda M_\Lambda}\rho_\Lambda^{5/3} \\ &+ (E_\Sigma + E_{\Sigma\Sigma} + E_{\Sigma\Lambda})\,\rho_\Sigma + \frac{C}{2m_\Sigma M_\Sigma}\rho_\Sigma^{5/3},\end{aligned} \tag{14}$$

with

$$E_N = (1-\beta)\,(a_0\rho_N + b_0\rho_N^{c_0}) + \beta\,(a_1\rho_N + b_1\rho_N^{c_1}), \tag{15a}$$

$$E_Y = (a_Y^0 + a_Y^1 x + a_Y^2 x^2)\rho_N + (b_Y^0 + b_Y^1 x + b_Y^2 x^2)\rho_N^{c_Y}, \tag{15b}$$

$$E_{YY'} = a_{YY'}\rho_N^{c_{YY'}}\rho_{Y'}^{d_{YY'}}, \tag{15c}$$

$$M_Y = 1 + \left(c_Y^0 + c_Y^1 x\right)\rho_N, \tag{15d}$$

where $\rho_N = \rho_n + \rho_p$; $x = \rho_p/\rho_N$; $\beta = (1-2x)^2$; $Y, Y' = \Lambda, \Sigma$, and $C = (3/5)(3\pi^2)^{2/3} \approx 5.742$. Here ε and ρ_i are given in units of $\mathrm{MeV\,fm}^{-3}$ and fm^{-3}, respectively (and $m_{\Lambda,\Sigma}$ in $\mathrm{MeV}^{-1}\,\mathrm{fm}^{-2}$).

Technically, these parametrizations were obtained by performing about 10^3 BHF calculations in the $(\rho_n, \rho_p, \rho_\Lambda, \rho_\Sigma)$-space, yielding "data" points $\varepsilon(\rho_n, \rho_p, \rho_\Lambda, \rho_\Sigma)$. The optimal values of the fit parameters were then determined hierarchically, first for nuclear matter, and then for hypernuclear matter, so that the fits are optimized also for pure nuclear matter. The optimal parameters are listed in table 3 for the V18+TBF+ESC08 model with (NY+YY) and without (NY) the effect of YY interactions that we compare in this article. The final overall r.m.s. deviation of fit and BHF data points for $E/A = \varepsilon/\rho$ is less than 1.8 MeV, which we consider fully satisfactory for our current purposes.

4.2 Effect of YY interactions

In order to analyze the effect of the YY interactions, it is useful to visualize the different contributions to the s.p. potentials in hypernuclear matter $U_B^{(B')}(k)$, eq. (9). Figure 3 displays this information for hypernuclear matter of nuclear density $\rho_N = 0.4\,\mathrm{fm}^{-3}$, proton fraction $\rho_p/\rho_N = 0.2$ (typical for a NS environment), and varying Λ (upper panel) or Σ^- (lower panel) fractions.

It is worth to note that at this density the Λ well depth is still very attractive, $U_\Lambda^0 \equiv U_\Lambda(k=0) \approx -40\,\mathrm{MeV}$, whereas $U_{\Sigma^-}^0 \approx +150\,\mathrm{MeV}$ is strongly repulsive and also $U_{\Xi^-}^0 \approx +40\,\mathrm{MeV}$ is repulsive. At normal nuclear density $\rho_N = 0.17\,\mathrm{fm}^{-3}$ and $\rho_p/\rho_N = 0.5$, $\rho_Y/\rho_N = 0$, the values $U_\Lambda^0 = -39\,\mathrm{MeV}$, $U_{\Sigma^-}^0 = +16\,\mathrm{MeV}$, $U_{\Xi^-}^0 = -8\,\mathrm{MeV}$ are compatible with current hypernuclear phenomenology [6] and have been used as constraints to fit the parameters of the ESC08 model.

The hatched areas in the upper panel show the contributions $U_B^{(\Lambda)}(k)$; $B = n, p, \Lambda, \Sigma$ and thus predominantly the effect of the $\Lambda(n, p, \Lambda, \Sigma)$ interactions in the hypernuclear environment. One notes attractive $\Lambda(n, p)$ and overall repulsive $\Lambda\Lambda$, but strongly attractive $\Lambda\Sigma$ interactions. In the same way the lower panel demonstrates repulsive $\Sigma^-\Sigma^-$ and $\Sigma^-(n, p)$ interactions. Obviously these global effects are the outcome of the interplay between the different coupled interaction channels, eq. (2).

The overall effect of YY interactions on the hypernuclear EOS therefore results from a competition between the $\Lambda\Lambda$, $\Sigma\Sigma$, and $\Lambda\Sigma$ channels, depending on the composition of the matter. In the presence of only one hyperon species the overall effect would be repulsive, whereas the coexistence of Λ and Σ^- implies a delicate balance of the attractive and repulsive effects, depending on the details of the interaction. If the beta-stable matter is dominated by the Λ, as is the case with the ESC08 model, one would expect an overall stiffening effect due to the repulsive in-medium $\Lambda\Lambda$ interaction.

This is indeed the case, as demonstrated in fig. 4, that shows in the upper panel the particle fractions $x_i \equiv \rho_i/\rho$,

Table 3. Fit parameters for the energy density of hypernuclear matter, eqs. (14) and (15), obtained with the V18+TBF+ESC08 potentials.

	V18+TBF+ESC08(NY)							V18+TBF+ESC08(NY+YY)						
$a_0\ b_0\ c_0\ a_1\ b_1\ c_1$	−140.7	390.1	2.08	88.3	634.3	3.11		−140.7	390.1	2.08	88.3	634.3	3.11	
$a_\Lambda^0\ a_\Lambda^1\ a_\Lambda^2\ b_\Lambda^0\ b_\Lambda^1\ b_\Lambda^2\ c_\Lambda$	−625	67	0	656	−17	0	1.28	−1047	122	0	1179	−85	0	1.19
$a_\Sigma^0\ a_\Sigma^1\ a_\Sigma^2\ b_\Sigma^0\ b_\Sigma^1\ b_\Sigma^2\ c_\Sigma$	−1285	−395	0	1856	−93	0	1.07	−198	−969	0	725	610	0	1.22
$a_{\Lambda\Lambda}\ c_{\Lambda\Lambda}\ d_{\Lambda\Lambda}$	218	0.95	0.84					372	0.26	1.37				
$a_{\Lambda\Sigma}\ c_{\Lambda\Sigma}\ d_{\Lambda\Sigma}$	0	0	0					1302	1.14	4.00				
$a_{\Sigma\Sigma}\ c_{\Sigma\Sigma}\ d_{\Sigma\Sigma}$	0	0	0					424	0.50	0.97				
$a_{\Sigma\Lambda}\ c_{\Sigma\Lambda}\ d_{\Sigma\Lambda}$	157	0.95	0.80					1047	1.49	1.52				
$c_\Lambda^0\ c_\Lambda^1\ c_\Sigma^0\ c_\Sigma^1$	−0.13	1.76	−0.75	−0.44				0.18	2.78	−0.60	−0.54			

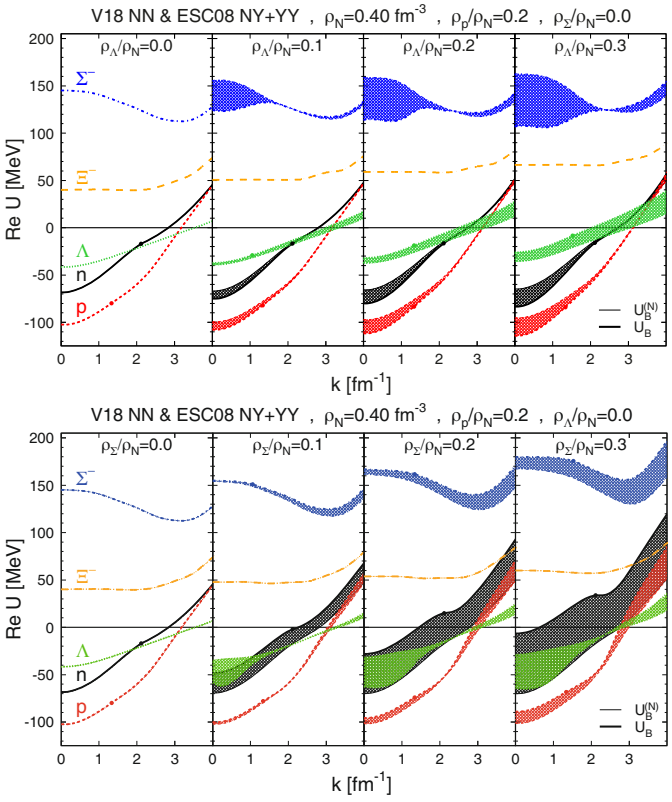

Fig. 3. Single-particle potentials of the different species $n, p, \Lambda, \Sigma^-, \Xi^-$ in nuclear matter of nuclear density $\rho_N = 0.4\,\mathrm{fm}^{-3}$, proton fraction $\rho_p/\rho_N = 0.2$, and varying Λ fraction (upper panel) or Σ^- fraction (lower panel). The dots indicate the positions of the Fermi momenta. Thin curves show results without effect of the YY interactions, whereas thick curves are the full results.

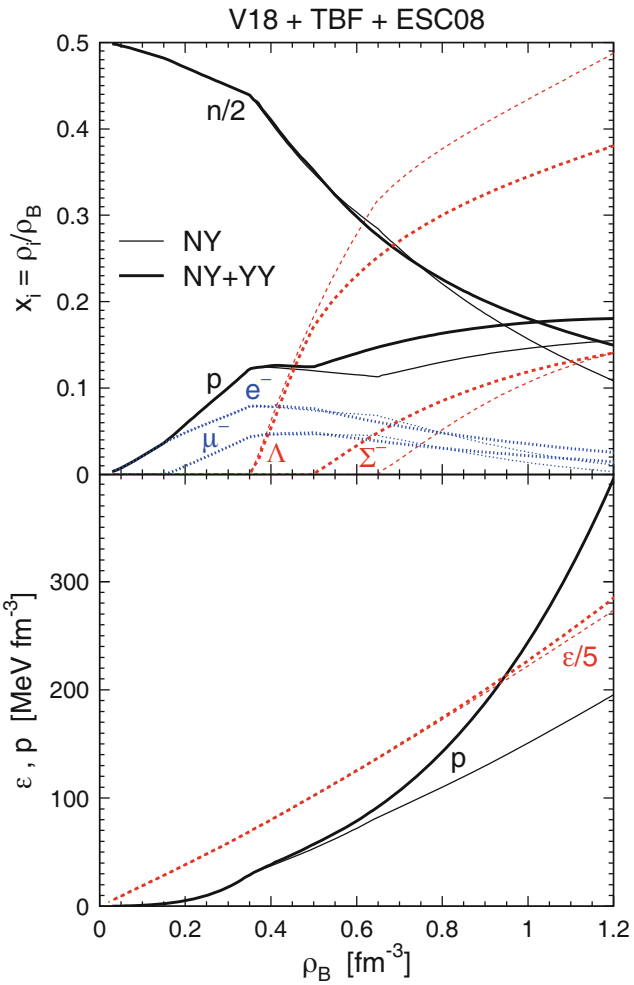

Fig. 4. Particle fractions (upper panel) and EOS (lower panel) of beta-stable NS matter obtained including (thick curves) or not (thin curves) YY interactions.

$i = n, p, \Lambda, \Sigma^-, e^-, \mu^-$; and in the lower panel the EOS $p(\rho), \varepsilon(\rho)$ of beta-stable NS matter. Comparing the results obtained including or not YY interactions (thick *vs.* thin curves), one notes clearly the dominant effect of the repulsive $\Lambda\Lambda$ interaction that reduces strongly the Λ concentration at high density. The attractive $\Lambda\Sigma^-$ interaction causes an earlier onset of the Σ^-, but the Σ^- concentration remains small, also because the repulsive $\Sigma^-\Sigma^-$ interaction becomes operative. The overall result is a stiffening of the EOS $p(\rho)$, as clearly seen in the lower panel of the figure. This obviously affects the predictions for the NS mass-radius relations that we discuss next.

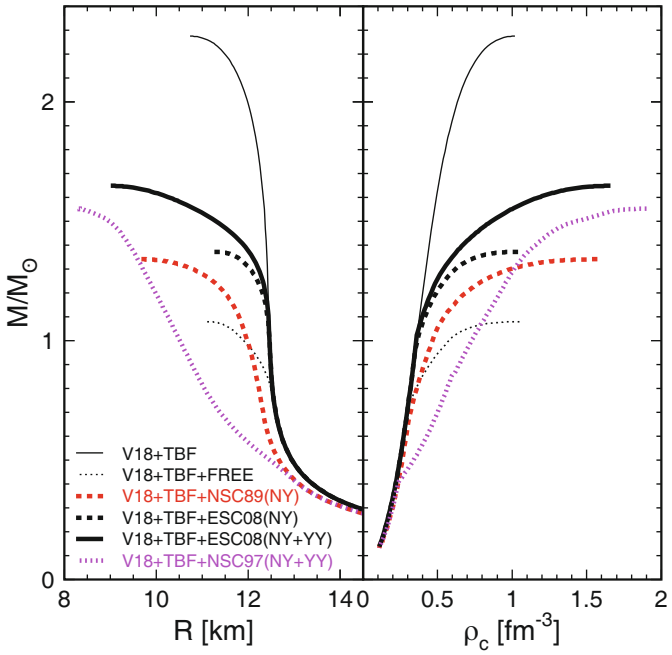

Fig. 5. Mass-radius and mass-central density relations for different equations of state. Details are given in the text.

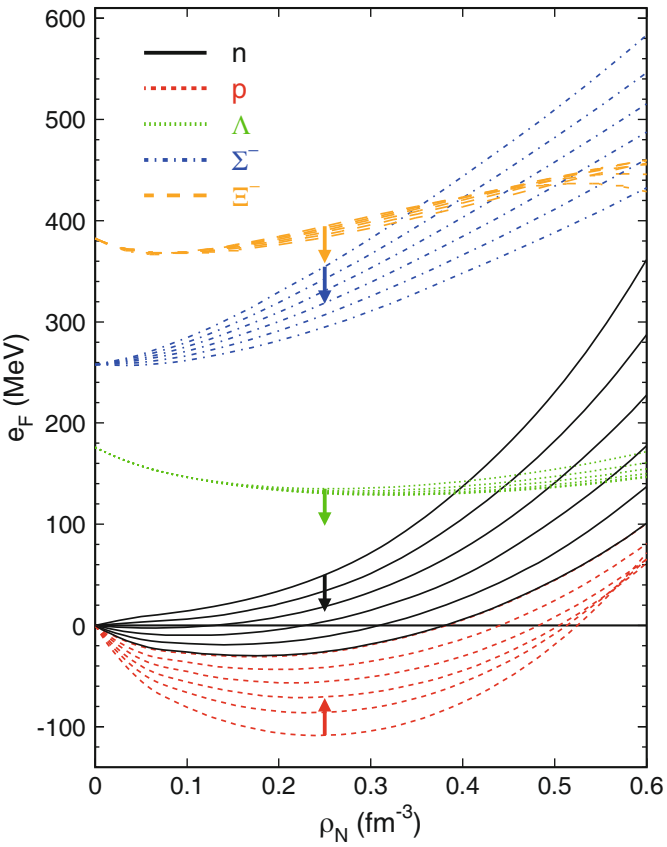

Fig. 6. Fermi energies, eq. (16), of the species $n, p, \Lambda, \Sigma^-, \Xi^-$ in asymmetric nuclear matter of density $\rho_N = \rho_n + \rho_p$ and proton fractions $x_p = \rho_p/\rho_N = 0.0, 0.1, 0.2, 0.3, 0.4, 0.5$ (increasing x_p indicated by the arrows).

4.3 Neutron star structure

Figure 5 compares the mass-radius and mass-central density relations obtained with the V18+TBF NN interaction and different choices for the NY and YY interactions. While excluding hyperons (thin solid curves) large masses ($2.3M_\odot$) can be reached, including them with only the NY interaction (black dashed curves) leads to a very strong reduction of the maximum mass to below $1.4M_\odot$. For comparison also the result without any NY interaction, counting only the Λ and Σ kinetic energies, are shown (thin dotted curves), featuring an extremely low maximum mass below $1.1M_\odot$. The NY interactions act thus overall repulsive at high density. In this case a large fraction of the NS core is composed of hyperons, which do not interact with each other, and therefore their fraction increases unimpeded with increasing baryon density. For this reason the maximum mass is nearly independent of the NY interaction, as demonstrated by the results obtained with the NSC89 NY interaction [1,21] shown for comparison (red dashed curves).

Activating the YY interactions has an overall repulsive effect, stiffening the EOS, as discussed in the previous section. Consequently the maximum mass increases to above $1.6M_\odot$ (black solid curves). Obviously this result depends on the details of the YY interactions, as demonstrated by comparing with an older result employing the NSC97 NY+YY forces [21] (magenta dotted curves), which yield a slightly smaller increase of the maximum mass to about $1.5M_\odot$. This is mainly because the NSC97 model predicts unrealistically attractive Σ^- s.p. potentials [20], and therefore this result cannot be considered realistic.

Clearly thus the features of the YY interactions affect the prediction of the NS maximum mass, even though a dramatic effect cannot be expected, also because we did not consider the remaining hyperons $\Sigma^0, \Sigma^+, \Xi^-, \Xi^0$, which could compensate for lower concentrations of Λ and Σ^- in the beta-stable matter. It is therefore clearly necessary to provide YY potentials as realistic as possible and well constrained by all possible experimental results.

4.4 Properties of Ξ^- in nuclear matter

In order to analyze somewhat more quantitatively the last aspect, namely the possible onset of the Ξ^- in NS matter, we display in fig. 6 the Fermi energies

$$e_F \equiv m - m_N + k_F^2/2m + U(k_F), \qquad (16)$$

of the various species in asymmetric nuclear matter of different proton fractions.

Assuming that the rearrangement corrections in the relation $\mu = e_F + \delta\mu_{\rm rearr.}$ are small [18,19], the plot can thus be used to estimate roughly the onset of the various hyperons in nuclear matter. For example, the Λ onset according to the condition $\mu_\Lambda = \mu_n$ occurs approximately at $\rho_N \approx 0.4\,{\rm fm}^{-3}$ (for $x_p \approx 0.1$), which is indeed the case in fig. 4.

More importantly, the onset of Ξ^- and Σ^- is determined by the common condition $\mu_{\Xi^-} = \mu_{\Sigma^-} = 2\mu_n - \mu_p$. From the figure one notes that for small proton fractions already at $\rho_N \approx 0.4\,\mathrm{fm}^{-3}$ the Ξ^- chemical potential becomes lower than the Σ^- one, overcoming their mass difference. Therefore from this point on the Ξ^- would be the preferred particle in NS matter and decrease the maximum mass even more than is the case in the previous study comprising only the Σ^-. The reason is the much more attractive $N\Xi^-$ interaction compared to $N\Sigma^-$.

However, the effects of the $S = -3$ $\Lambda\Xi^-$ and $S = -4$ $\Xi^-\Xi^-$ interactions are not included in this analysis. An accurate treatment of the phenomenon therefore requires yet more complex calculations including even the $S = -3, -4$ interaction channels. For the moment this is beyond our capabilities, both regarding possible experimental constraints for the relevant potentials, and performing the extended BHF calculations including the three hyperons Λ, Σ^-, Ξ^- simultaneously. In any case a further reduction of the maximum mass is expected.

5 Conclusions and prospects

In this article the finding of very low maximum masses of hyperon stars within the BHF approach is reconfirmed, using the recent realistic ESC08 NY and YY interactions for the strangeness $S = -1, -2$ baryon-baryon channels.

We have elucidated the intricate effects of the coupled YY interaction channels in hypernuclear matter, which at high density turn out repulsive in the $\Lambda\Lambda$ and $\Sigma\Sigma$ and attractive in the $\Lambda\Sigma$ channels. Their overall effect is repulsive with the ESC08 model and increases the maximum mass by $0.3M_\odot$ to about $1.65M_\odot$, still far from the current observational limit $> 2M_\odot$. Also, the expected onset of the Ξ^- will reduce the maximum mass again.

Thus, for those massive NS, either some strong TBF repulsion from, *e.g.*, a QCD origin could be operative [41–43], and/or they have to be hybrid stars containing a core of non-baryonic ("quark") matter [56–63].

As we have discussed above, the ESC approach is a model which can provide consistent baryon-baryon and quark-quark interactions. Such a model could be applied to the required global treatment of the combined baryon and quark phase. For example, the multi-pomeron exchange has the form of a contact interaction. Assuming that short-range interactions will be the dominant ones for high density, also the ESC meson-exchange potential could be reduced to contact interactions in the form of some generalized Nambu–Jona-Lasinio model [64–66]. It will be an important task for the future to verify this assertion by following the experimental and theoretical developments in this field.

We thank E. Hiyama and Y. Yamamoto for useful discussions. Partial support comes from "NewCompStar," COST Action MP1304, and from the Munich Institute for Astro- and Particle Physics (MIAPP) of the DFG cluster of excellence "Origin and Structure of the Universe."

References

1. H.-J. Schulze, T. Rijken, Phys. Rev. C **84**, 035801 (2011).
2. T. Rijken, M. Nagels, Y. Yamamoto, Nucl. Phys. A **835**, 160 (2010).
3. Y. Yamamoto, E. Hiyama, T. Rijken, Nucl. Phys. A **835**, 350 (2010).
4. T. Rijken, M. Nagels, Y. Yamamoto, Prog. Theor. Phys. Suppl. **185**, 14 (2010).
5. Y. Yamamoto, T. Motoba, T. Rijken, Prog. Theor. Phys. Suppl. **185**, 72 (2010).
6. M.M. Nagels, Th.A. Rijken, Y. Yamamoto, arXiv: 1408.4825 (2014), 1501.06636 (2015), 1504.02634 (2015).
7. P.B. Demorest, T. Pennucci, S.M. Ransom, M.S.E. Roberts, J.W.T. Hessels, Nature **467**, 1081 (2010).
8. J.A. Antoniadis *et al.*, Science **340**, 6131 (2013).
9. S.L. Shapiro, S.A. Teukolsky, *Black Holes, White Dwarfs and Neutron Stars* (Wiley, New York, 1983).
10. N.K. Glendenning, *Compact Stars: Nuclear Physics, Particle Physics and General Relativity*, 2nd edition (Springer, Berlin, 2000).
11. H. Heiselberg, M. Hjorth-Jensen, Rep. Rep. **328**, 237 (2000).
12. J. Schaffner-Bielich, J. Phys. **G 31**, S651 (2005).
13. J. Schaffner-Bielich, Nucl. Phys. A **804**, 309 (2008).
14. H.Q. Song, M. Baldo, G. Giansiracusa, U. Lombardo, Phys. Rev. Lett. **81**, 1584 (1998).
15. M. Baldo, G. Giansiracusa, U. Lombardo, H.Q. Song, Phys. Lett. B **473**, 1 (2000).
16. M. Baldo, A. Fiasconaro, H.Q. Song, G. Giansiracusa, U. Lombardo, Phys. Rev. C **65**, 017303 (2001).
17. H.-J. Schulze, M. Baldo, U. Lombardo, J. Cugnon, A. Lejeune, Phys. Rev. C **57**, 704 (1998).
18. M. Baldo, G.F. Burgio, H.-J. Schulze, Phys. Rev. C **58**, 3688 (1998).
19. M. Baldo, G.F. Burgio, H.-J. Schulze, Phys. Rev. C **61**, 055801 (2001).
20. I. Vidana, A. Polls, A. Ramos, M. Hjorth-Jensen, V.G.J. Stoks, Phys. Rev. C **61**, 025802 (2000).
21. H.-J. Schulze, A. Polls, A. Ramos, I. Vidana, Phys. Rev. C **73**, 058801 (2006).
22. Z.H. Li, H.-J. Schulze, Phys. Rev. C **78**, 028801 (2008).
23. G.F. Burgio, H.-J. Schulze, Phys. Rev. C **73**, 058801 (2006).
24. G.F. Burgio, H.-J. Schulze, Astron. Astrophys. **518**, A17 (2010).
25. G.F. Burgio, H.-J. Schulze, A. Li, Phys. Rev. C **83**, 025804 (2011).
26. M. Baldo, I. Bombaci, G.F. Burgio, Astron. Astrophys. **328**, 274 (1997).
27. M. Baldo, L.S. Ferreira, Phys. Rev. C **59**, 682 (1999).
28. X.R. Zhou, G.F. Burgio, U. Lombardo, H.-J. Schulze, W. Zuo, Phys. Rev. C **69**, 018801 (2004).
29. P. Grange, A. Lejeune, M. Martzolff, J.-F. Mathiot, Phys. Rev. C **40**, 1040 (1989).

30. W. Zuo, A. Lejeune, U. Lombardo, J.-F. Mathiot, Nucl. Phys. A **706**, 418 (2002).
31. W. Zuo, A. Lejeune, U. Lombardo, J.-F. Mathiot, Eur. Phys. J. A **14**, 469 (2002).
32. Z.H. Li, U. Lombardo, H.-J. Schulze, W. Zuo, Phys. Rev. C **77**, 034316 (2008).
33. R.B. Wiringa, V.G.J. Stoks, R. Schiavilla, Phys. Rev. C **51**, 38 (1995).
34. B.S. Pudliner, V.R. Pandharipande, J. Carlson, S.C. Pieper, R.B. Wiringa, Phys. Rev. C **56**, 1720 (1997).
35. A. Akmal, V.R. Pandharipande, G. Ravenhall, Phys. Rev. C **58**, 1804 (1998).
36. P.M.M. Maessen, Th.A. Rijken, J.J. de Swart, Phys. Rev. C **40**, 2226 (1989).
37. V.G.J. Stoks, Th.A. Rijken, Phys. Rev. C **59**, 3009 (1999).
38. V.G.J. Stoks, R.A.M. Klomp, M.C.M. Rentmeester, J.J. de Swart, Phys. Rev. C **48**, 792 (1993).
39. H. Takahashi *et al.*, Phys. Rev. Lett. **87**, 212502 (2001).
40. Th.A. Rijken, *Constituent Quark Meson-exchange Interactions*, preprint Radboud University Nijmegen 2015, in preparation.
41. Y. Yamamoto, T. Furumoto, N. Yasutake, Th.A. Rijken, Phys. Rev. C **88**, 022801 (2013).
42. Y. Yamamoto, T. Furumoto, N. Yasutake, Th.A. Rijken, Phys. Rev. C **90**, 045805 (2014).
43. Y. Yamamoto, T. Furumoto, N. Yasutake, Th.A. Rijken, Eur. Phys. J. A **52**, 19 (2016).
44. T. Fukuda *et al.*, Phys. Rev. C **58**, 1306 (1998).
45. P. Khaustov *et al.*, Phys. Rev. C **61**, 054603 (2000).
46. R.H. Dalitz, D.H. Davis, P.H. Fowler, A. Montwill, J. Pniewski, J.A. Zakrewski, Proc. R. Soc. A **426**, 1 (1989).
47. Th.A. Rijken, V.G.J. Stoks, Y. Yamamoto, Phys. Rev. C **59**, 21 (1999).
48. D'Agostini *et al.*, Rome-Saclay-Vanderbilt collaboration, Nucl. Phys. B **209**, 1 (1982).
49. T. Inoue *et al.*, Phys. Rev. Lett. **106**, 162002 (2011).
50. T. Inoue *et al.*, Nucl. Phys. A **881**, 28 (2012).
51. R.L. Jaffe, Phys. Rev. Lett. **38**, 195,617 (1977).
52. B.H. Kim *et al.*, arXiv:1302.4028v1 (2013).
53. J.W. Negele, D. Vautherin, Nucl. Phys. A **207**, 298 (1973).
54. R.P. Feynman, N. Metropolis, E. Teller, Phys. Rev. **75**, 1561 (1949).
55. G. Baym, C. Pethick, P. Sutherland, Astrophys. J. **170**, 299 (1971).
56. G.F. Burgio, M. Baldo, P.K. Sahu, H.-J. Schulze, Phys. Rev. C **66**, 025802 (2002).
57. M. Baldo, M. Buballa, G.F. Burgio, F. Neumann, M. Oertel, H.-J. Schulze, Phys. Lett. B **562**, 153 (2003).
58. C. Maieron, M. Baldo, G.F. Burgio, H.-J. Schulze, Phys. Rev. D **70**, 043010 (2004).
59. M. Baldo, G.F. Burgio, P. Castorina, S. Plumari, D. Zappala, Phys. Rev. C **75**, 035804 (2007).
60. T. Maruyama, S. Chiba, H.-J. Schulze, T. Tatsumi, Phys. Rev. D **76**, 123015 (2007).
61. H. Chen, M. Baldo, G.F. Burgio, H.-J. Schulze, Phys. Rev. D **84**, 105023 (2011).
62. H. Chen, J.-B. Wei, M. Baldo, G.F. Burgio, H.-J. Schulze, Phys. Rev. D **91**, 105002 (2015).
63. A. Kurkela, P. Romatschke, A. Vuorinen, Phys. Rev. D **81**, 105021 (2010).
64. M. Buballa, S. Krewald, Phys. Lett. B **294**, 19 (1992).
65. N. Yasutake, R. Lastowiecki, S. Benic, D. Blaschke, T. Maruyama, T. Tatsumi, Phys. Rev. C **89**, 065803 (2014).
66. S. Benic, D. Blaschke, G.A. Contrera, D. Horvatic, Phys. Rev. D **89**, 016007 (2014).